Evaluation of the contribution of new particle formation to cloud droplet number concentration in urban atmosphere

Sihui Jiang[1], Fang Zhang[1*], Jingye Ren[1], Lu Chen[1], Xing Yan[1], Jieyao Liu[1], Yele Sun[2], Zhanqing Li[3]

[1]College of Global Change and Earth System Science, Beijing Normal University, Beijing 100875, China

[2]State Key Laboratory of Atmospheric Boundary Layer Physics and Atmospheric Chemistry, Institute of Atmospheric Physics, Chinese Academy of Sciences, Beijing, China

[3]Earth System Science Interdisciplinary Center and Department of Atmospheric and Oceanic Science, University of Maryland, College Park, Maryland, USA

Correspondence to: F. Zhang, *fang.zhang@bnu.edu.cn;*

Abstract

The new particle formation (NPF) effect on cloud condensation nuclei (CCN) varies widely in diverse environment. The CCN or cloud droplet from NPF sources remains highly uncertain in urban atmosphere which are greatly affected by the high background aerosols and frequent local emissions. In this study, we quantified the NPF effect on cloud droplet number concentration (CDNC, or N_d) at typical updraft velocities (V) in clouds based on field observations on May 25-June 18, 2017 in urban Beijing. We show that the NPF increases the N_d by 32-40% at V= 0.3-3 m s^{-1} during the studied period. The N_d is reduced by 11.8±5.0% at V=3 m s^{-1} and 19.0±4.5% at V=0.3 m s^{-1} compared to that calculated from constant supersaturations due to the water vapor competition effect, which suppress the cloud droplet formation by decreasing the environmental maximum supersaturation (S_{max}). The effect of water vapor competition becomes smaller at larger V that can provide more sufficient water vapor. However, under extremely high aerosol particle number concentrations, the effect of water vapor competition becomes more pronounced. As a result, although a larger increase of CCN-size particles by NPF event is derived on clean NPF day when the number concentration of pre-existing background aerosol particles is very low, no large discrepancy is presented in the enhancement of N_d by NPF between the clean and polluted NPF day. We finally reveal a considerable impact of the primary sources on the evaluation of the NPF contribution to N_{CCN} and N_d based on a case study. Our study highlights the importance of fully consideration of both the environmental meteorological conditions and multiple sources (i.e. secondary and primary) to evaluate the NPF effect on clouds and the associated climate effects in polluted regions.

1 Introduction

In the global climate system, aerosols, cloud condensation nuclei (CCN) and cloud droplets are very important components. Clouds, serving as a bridge connecting aerosols and climate, are the most uncertain factor of climate change (IPCC, 2013; Seinfeld et al., 2016; Cai et al., 2020). The microphysical link between aerosols and clouds as the most important part has received extensive attention. Cloud droplet activation is a key process from aerosol to clouds, and researchers have tried to simulate the microphysical processes by using numerical activation models (e.g. Boucher and Lohmann., 1995; Abdul-Razzak et al., 1998; Kiehl,1999; Khvorostyanov and Curry., 1999; Abdul-Razzak and Ghan., 2000; Nenes et al., 2002, 2004; Petters et al., 2007; Ren et al., 2018; Genz et al., 2020).

New particle formation events (NPF) have been observed and occurred frequently in different atmospheric environments in the world (Spracklen et al., 2010; Yue et al., 2011; Peng et al., 2017; Kerminen et al., 2018; Bousiotis et al., 2019; Zimmerman et al., 2020). The NPF events was one of the most significant sources of fine particles in the atmosphere (Shi et al., 1999; Stanier et al., 2004; Kulmala and Kerminen, 2008). For example, it has been found that the NPF contributed about 76% of the total fine particle number concentrations in urban Beijing (Wu et al., 2011). These nucleated particles subsequently grow through coagulation or condensation processes to CCN-relevant sizes, or act as CCN in convective clouds (Fan et al., 2013; Li et al., 2010). In reality, the field studies have shown that these fine particles produced from NPF can subsequently turn into an enhancement in N_{CCN} at cloud-relevant supersaturations (Kalkavouras et al., 2017; Peng et al., 2014; Wu et al., 2015; Ma et al., 2016; Li et al., 2017; Zhang et al., 2019). It was estimated that up to 80% of CCN number concentration (N_{CCN}) is from the nucleation process in urban Beijing (Wiedensohler et al., 2008).

However, the N_{CCN} only reflects the cloud forming potential of aerosol particles at a given supersaturation. The measurement of CCN is usually carried out at constant supersaturations. Different from the prescribed supersaturation used in the evaluation of N_{CCN}, when calculating the cloud droplet number concentration (CDNC, or N_d), researchers considered the dynamic situations in clouds. In clouds, the supersaturation exhibits variable levels that instantaneously adjust to the intensity of cloud updrafts and the particle number size distribution (PNSD) (Nenes et al., 2003; Hudson et al., 2015). So the CDNC, (or N_d) depends on the size distribution, chemical properties of aerosol and the cloud updraft velocity, all of which regulate the maximum supersaturation (S_{max}) that can be formed in a cloud parcel (Nenes and Seinfeld, 2003). Studies have shown that the CDNC in clouds exhibits a sublinear relationship to aerosol number concentration (N_{CN}) (Twomey, 1977; Leaitch et al., 1986; Ghan et al., 1993; Boucher and Lohmann, 1995; Nenes et al., 2001; Ramanathan et al., 2001; Sullivan et al., 2016), this is different from CCN due to the limitation of the water vapor in the actual environment. Using the prescribed supersaturation to calculate CDNC may therefore provide a bias on evaluation the aerosol indirect effect. For example, Kalkavouras et al. (2017, 2019) reported an average 12% enhancement of CDNC during two consecutive NPF episodes in the eastern Mediterranean, which was significantly smaller than the enhancement of N_{CCN} (~87%) during the NPF events. Hence, it is critical to fully consider the background meteorological conditions (e.g. using dynamic water vapor under different updraft velocities) to simulate the S_{max} when evaluating the effect of NPF on clouds and the associated climate effects.

Relevant studies have been carried out in clean regions, but fewer in polluted urban areas. While field studies have shown that NPF events can occur frequently in polluted urban sites although the high concentration of background particles are not conducive to the generation of new particles (Wu

et al., 2011; Peng et al., 2014; Zimmerman et al., 2020), and the formation and growth rate of new particles may be larger than that of relatively clean atmosphere. Wiedensohler et al. (2012) found that, under the high concentration levels of gaseous pollutants and strong oxidation in polluted area, the high concentration of nanoparticles generated by NPF events can rapidly grow to tens or even hundreds of nanometers in a few hours. Zhang et al. (2019) observed the subsequent growth of newly formed particles can last 2-3 days in urban Beijing, producing more CCN-sized particles. Previous studies in polluted regions demonstrated the complex and non-linear relationship between aerosol particles and CCN due to multiple emission sources (Zhang et al., 2014, 2016, 2017, 2019; Ren et al., 2018; Fan et al., 2020), highlighting the importance of understanding of the connections between aerosols and CCN or cloud droplet close to the source regions. Particularly, owing to the extremely high CN number concentrations (with order of magnitude as high as 10^4 or even 10^5 cm^{-3}) during NPF events in urban area, the effect of competition for water vapor and reduction in cloud supersaturation is expected to be more exacerbated.

The current study quantifies the contribution of NPF to N_{CCN} and CDNC in the polluted urban atmosphere of Beijing using field measurements of aerosol number size distributions and chemical composition. The effect of water vapor competition on evaluating N_d during NPF events is examined. The impact of the background pre-existing particles on the enhancement of CCN and CDNC is also discussed by contrasting the results on typical "clean" NPF day and "polluted" NPF day. Given the strong local primary sources like traffic emissions in urban area, a case study is conducted to investigate the impact of primary emissions on the evaluation of NPF effect on N_d.

2 Methodology

2.1 Site and experiment

A field campaign was conducted from May 25, 2017 to June 18, 2017 at the Institute of Atmospheric Physics (IAP), Chinese Academy of Sciences (39.98° N, 116.39° E) for measurements of aerosol physical and chemical properties. The IAP located between the north Third Ring Road and Fourth Ring Road in northern Beijing, which is a typical urban background site, mainly affected by traffic and cooking emissions. Beijing is hot in summer with high ambient relative humidity, which is conductive to generate atmospheric convection and reduce the high background aerosol condensation sink. The radiation in summer is stronger than other seasons, which promotes the generation of nucleated particles. Besides, local sources from traffic and cooking emissions, which may contribute many CCN size-relevant particles, can be important at the site (Sun et al., 2015). The instruments during the campaign were deployed in a container at ground level (~8 m on a meteorological tower).

The number size distribution of particles in the size range from 10 to 550 nm (scanned range) were measured with time resolution of 5 minutes by a scanning mobility particle sizer (SMPS; Wang and Flagan, 1990; Collins et al., 2002), which consists of a differential mobility analyzer (DMA, model 3081L, TSI Inc.) to classify particles with different sizes of particles, and a condensation particle counter (CPC, model 3772, TSI Inc.) to detect the size-classified particles. The sampled particles were dried to a relative humidity < 30% before entering the DMA. The non-refractory chemical composition of PM_1 is measured by an Aerosol Chemical Speciation Monitor (ACSM), which consists of an aerodynamic lens to efficiently sample and focus submicron particles into the ACSM (Ng et al. 2011). Before sampling into the ACSM, aerosol particles are dried by silica gel desiccant. The ACSM was operated at a time resolution of 15 min. And the non-refractory chemical

components that can be measured mainly include organics, sulfate salts (SO_4^{2-}), nitrate salts (NO_3^-), ammonium (NH_4^+), and chloride (Cl^-) (Ng et al. 2011). The refractory components mainly include black carbon (BC), and the BC mass concentration was measured using a seven-wavelength aethalometer (AE33, Magee Scientific Corp) .

2.2 Calculation of N_{CCN}

According to the hygroscopic growth process of particles described by Köhler theory (Köhler et al., 1936), the particles with the dry particle diameter (D_p) larger than the critical dry particle diameter (D_c) can be activated to form a cloud droplet. In this study, the κ-Köhler theory (Petters and Kreidenweis, 2007), which simply describe the approximate relationship between the D_c with the critical supersaturation (S_c), is applied as follows, when $\kappa > 0.1$:

$$K=\frac{4A^3}{27D_c^3 ln^2 S_c},\ A=\frac{4\sigma_w M_w}{RT\rho_w} \quad (1)$$

where M_w is the molecular weight of water (M_w = 0.018015 kg mol^{-1}), ρ_w is the density of water (ρ_w= 997.1 kg m^{-3}), T is the parcel temperature (T = 298.15 K), where σ_w is the droplet surface tension at the point of activation (σ_w = 0.072 J m^{-2}) and R is the universal gas constant (R = 8.315 J K^{-1} mol^{-1}). κ is a hygroscopic parameter which depends on the chemical composition of the particle. In this study, based on the assumption that particles are internally mixed and their chemical composition will not be impacted by changes in particle size, we derived the κ with a simple mixing rule on the basis of chemical volume fractions (Petters and Kreidenweis, 2007; Gunthe et al., 2009). We used ACSM data, combined with the positive matrix factorization (PMF) analysis data to calculate the volume fraction of organic and inorganic, according to the following equation:

$$\kappa_{chem}=\sum_i \varepsilon_i \kappa_i \quad (2)$$

where κ_i and ε_i are the hygroscopic parameter and volume fraction for each individual (dry)

component in the mixture, respectively. The κ value and density (ρ) of each species used in the calculation are given in Table 1, which is referred from Petters and Kreidenweis (2007) and Topping (2005).

Table 1. Densities of different chemical species and their κ measured by the laboratory

Species	NH_4NO_3	$(NH_4)_2SO_4$	NH_4HSO_4	H_2SO_4	POA*	SOA*	BC
ρ (kg m-3)	1720	1769	1780	1830	1000	1400	1700
κ	0.58	0.48	0.56	1.19	0	0.09	0

POA* refers to primary organic aerosol and SOA* refers to secondary organic aerosol

In the equation (1), the corresponding D_c can be obtained from a given S_c, and all particles with diameters larger than D_c can be activated. So the N_{CCN} can be calculated by integrating the PNSD from D_c to the largest particle size measured:

$$CCN(D_c) = \int_{D_c}^{550} n(logD_p) dlogD_p \quad (3)$$

where $n(logD_p)$ is the particle number that correspond to each particle size bin $dlogD_p$ in the aerosol number size distribution.

2.3 Calculation of N_d

The N_d depends on the S_{max} that can be formed in adiabatic ascending clouds. And this "cloud-relevant" supersaturation varies at different updraft velocity. A global scheme of cloud droplet parameterization has been established and developed for the calculation of the N_d and S_{max} (Nenes and Seinfeld, 2002, 2004; Fountoukis and Nenes, 2005). In this study, the S_{max} was calculated from an equation that expresses the water vapor balance in adiabatic ascending cloud (Nenes and Seinfeld., 2003):

$$\frac{ds}{dt} = \alpha V - \gamma \frac{dw}{dt} \quad (4)$$

where α and γ are two coefficients can be calculated by meteorological constants, the product of α and V expresses the increase of supersaturation due to the adiabatic cooling of the parcel, while the

$\frac{dw}{dt}$ denotes the water condensation rate during the aerosol activation and subsequent growth processes. which is shown in detail in Eqs (5). And the $\frac{ds}{dt}$ express the growth rate of supersaturation, when it is equal to 0, the supersaturation reaches the maximum value.

$$\frac{dw}{dt} = \frac{\pi}{2}\rho_w \int_0^S D_p^2 \frac{dD_p}{dt} n^S(S')dS' \quad (5)$$

where ρ_w is the density of water. $n^s(S')dS'$ is the number concentration of particles activated between S' and $S' + dS$.

Nenes et al.(2002) used a sectional representation of the CCN spectrum (i.e. particle number supersaturation distribution $n^s(s')$) and total number of particles with S_c smaller than S, $F^S(S)$, which is given by

$$F^S(S_x) = \int_0^{S_x} n^S(S')dS' \quad (6)$$

Where the S_x is the supersaturation in the environment, the $n^S(S')$ in equation (6) represents the number concentration of particles activated between S' and $S' + dS'$ in CCN spectrum. The $F^S(S_x)$ can be calculated by the integration of $n^S(S')$ from the lower limit 0 to upper limit S_x. If the S_{max} is known, the activated N_d can be calculated from equation (7), as

$$N_d = F^S(S_{max}) \quad (7)$$

In this study, we used the PNSD, chemical components, and empirical values of cloud updraft velocity to determine the S_{max} and N_d during NPF days in urban Beijing. Owing to that the direct measurement of cloud-scale updraft velocity in the atmosphere is almost impossible, the prescribed updraft velocity used in this study is referred from previous studies. Generally, the updraft velocities are reported very small (Martin et al., 1994) and range from 0.1 to 1.0 m/s in stratocumulus and cumulus clouds in remote or marine boundary layer (Meskhidze et al., 2005; Morales et al., 2010). The vertical updraft velocities were derived varying from 0.3 to 3 m/s (Zheng et al., 2015), which are

typical for cumulus and convective clouds in summer of north China and thus was selected and applied in this study.

2.4 Method for calculating the contribution of NPF to N_{CCN} and N_d

The increment of N_{CCN} or N_d by the NPF (ΔN_{CCN} or ΔN_d) is usually quantified by comparing the N_{CCN} or N_d prior and after the NPF event (Peng et al., 2014; Wu et al., 2015; Ma et al., 2016; Ren et al., 2018; Zhang et al., 2019; Fan et al., 2020). In this study, the N_{CCN} or N_d prior the NPF event was determined as two-hours average of N_{CCN} or N_d before the burst of newly formed nucleated particles. And the N_{CCN} and N_d after the NPF event was calculated as the average of N_{CCN} or N_d from begin to the end of the NPF impact the N_{CCN} or N_d. So it is critical to determine when a NPF event start and end, or when a NPF begins and ends the impact on the N_{CCN} or N_d.

Generally, the burst in the nucleation mode particles symbolizes the beginning of an NPF event. Here, the moment when a half-hour concentration of the nucleation-mode particles suddenly increases with order of magnitude as high as ~10^4 cm^{-3} during NPF cases was defined as t_{start}. The end time of an NPF event, t_{end}, is defined by the moment when the half-hour concentrations of nucleated particle is lower than that at t_{start}.

Since there need some time for the newly formed nucleated particles to grow to sufficient size to act as CCN, the N_{CCN} would not be enhanced as soon as new particles are generated. To determine the time that NPF begins and end the impact on the N_{CCN}, denoted as $t_{start,CCN}$ and $t_{end,CCN}$ respectively, the time series of N_{CCN} was firstly divided by the N_{CCN} at t_{start} at each prescribed supersaturation, to derive the normalized time series of N_{CCN}, denoted as R_s. The equation is written as follows,

$$R_S = \frac{CCN_S}{CCN_{S,t_{start}}} \quad (8)$$

where S represents the supersaturation. Before the new particles reaches a large enough size to impact N_{CCN}, the variations of R_S should remain constant for different supersaturations if the concentrations of the background or pre-exist aerosols changes insignificant. And at $t_{start,CCN}$ when NPF begin to impact the N_{CCN}, an apparent increase in R_S is observed by taking the observation on June 11 as an example (Fig. 1a). Also, due to the heterogenous composition and distinct CCN activity of the newly formed particles (Duan, et al., 2018; Ren et al., 2018; Zhang et al., 2019; Tao, et al., 2021;), a parameter, R_D, which was calculated with the relative standard deviation of the R_S of different supersaturations at a given time, is applied to fix the $t_{start,CCN}$ and $t_{end,CCN}$. Then the $t_{start,CCN}$ and $t_{end,CCN}$ correspond to the moments when the R_D starts to increase and back to nearly zero (Fig. 1b) respectively between the t_{start} and t_{end}. The same method is used to determine the time that NPF begins and ends the impact on the N_d, which are denoted as t_{start,N_d} and t_{end,N_d} respectively (Fig. 1d, e). More details about the method can be found in Kalkavouras et al. (2019). As shown in Fig. 1, it is clearly that both the N_{CCN} and N_d exhibits large increase in the NPF-impacted time zone between $t_{start,CCN}$ and $t_{end,CCN}$ (Fig. 1c), and between t_{start,N_d} and t_{end,N_d} (Fig. 1f). The average time lag between t_{start} and t_{start,N_d} was about 3-5 hours which is shortened by 50% compared to that reported by Kalkavouras et al., (2019). This case on 11 June was not an individual case, and similar patterns are also shown on other NPF days during the campaign (Fig. S3-S8).

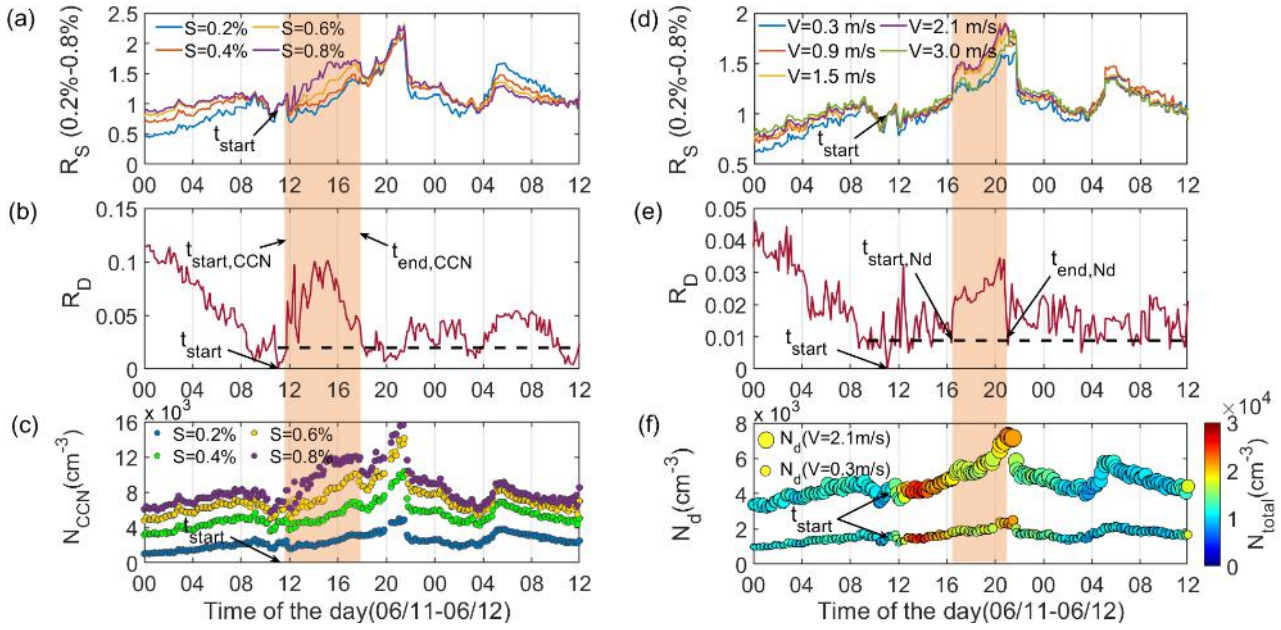

Figure 1. The diurnal evolution of (a) the R_S of N_{CCN} at different supersaturations, (b) the relative dispersion of R_S, R_D, for N_{CCN} at different supersaturations, (c) the calculated N_{CCN} under different supersaturations, (d) the R_S of N_d under updraft velocities from 0.3 to 3.0 m/s, (e) the R_D for N_d, and (f) the calculated N_d at updraft velocities of 0.3 and 2.1 m/s on 11 June, 2017.

Note that this method is with an assumption of the unchanged background pre-exist aerosols during the NPF events, without consideration of the impacts from local emission sources, and diurnal changes in the planetary boundary layer (PBL). As shown in Fig. 2b, the time series of N_{CN} presents a baseline which indicates that concentrations of the background aerosols on each of the 7 typical NPF day don't vary much, the impact from the variation of background aerosol particles thus should be insignificant. The impact of PBL is expected to be small when the growth of the newly formed particles spans only a few hours. However, when the growth continues longer time to evening or at night which may coincide with the period that the PBL height changes from high to low (Kerminen et al., 2012; Altstädter, et al., 2015; Li et al., 2017), it will result in a larger N_{CCN} and N_d, leading to an overestimation of the contribution of NPF to N_{CCN} and N_d. A quantitative evaluation of such impact is difficult due to that the contemporary PBL data is not available. Therefore, here we only

investigate the impact of local emissions on the evaluation of NPF effect on N_d based on a case study.

3 Results and discussion

3.1 Time series of observed NPF events and calculated N_{CCN} and N_d

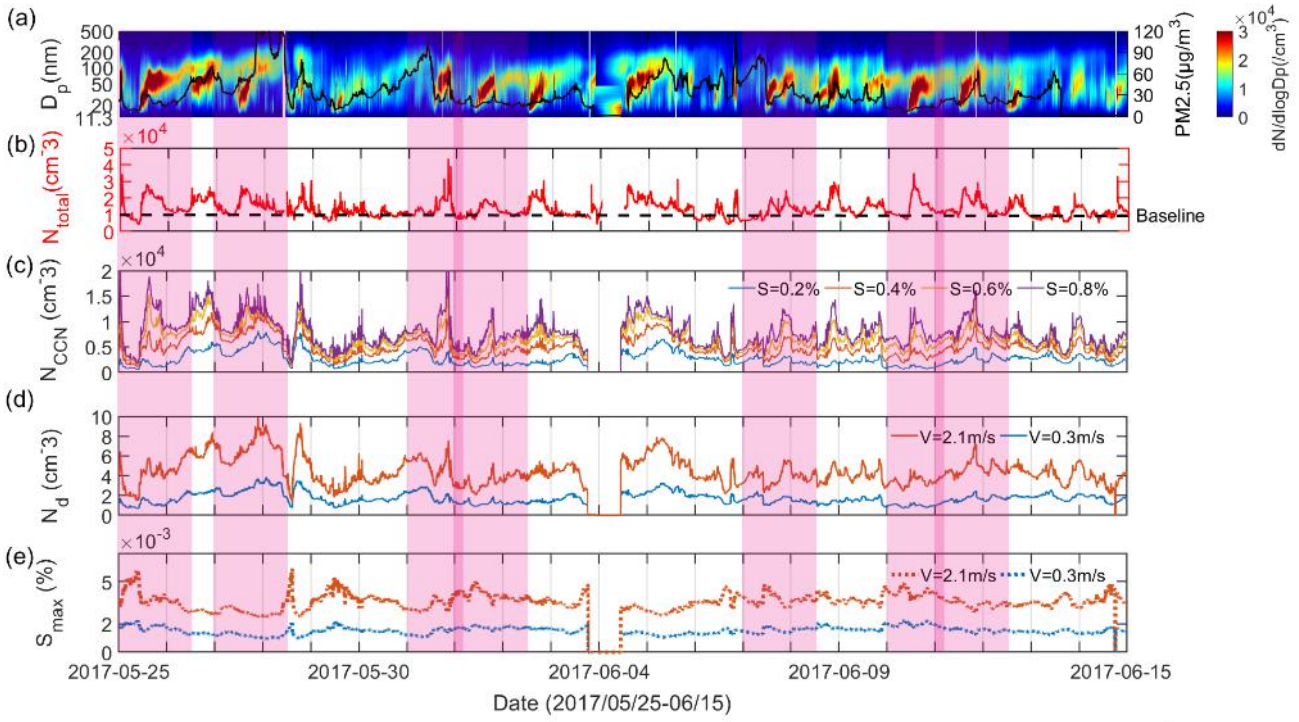

Figure 2. Time series of (a) particle number size distribution (PNSD) (the selected 7 typical NPF events are marked in pink shadow), (b) the total particle number concentration (N_{total}), (c) CCN number concentration (N_{CCN}), (d) cloud droplets number concentration (N_d) and (e) the maximum supersaturation (S_{max}) from 25 May to 15 June 2017.

During the observed periods from 25 May to 15 June 2017, the NPF events occurred on most of days (~13 days) (Fig. 2a). According to Dal Maso et al., (2005) and Wu et al., (2015), a typical NPF event includes the sudden appearance and continuous growth of particles smaller than 25 nm, and a "banana" shape can be seen on the particle number size spectrum. While non-NPF events may also have sudden increases of fine particles at a short time scale (e.g. local sources from vehicle or cooking emissions), but they do not show the "banana" shape. Therefore, those cases with typical

269 "banana" shape (7 NPF events in total), which presents a complete NPF evolution process from
270 nucleation to subsequent growth (not interrupted by meteorological conditions either), are selected
271 for further study (marked in pink shadow in Fig. 2). Fig. 2b, c and d present the time series of N_{CN},
272 N_{CCN} and N_d. It exhibits that the NPF event drives the variation of N_{CCN} and N_d, showing that the
273 occurrence of NPF events as an important source of CCN. The variation trend of N_{CN} is more
274 correlated with that of N_{CCN} than N_d (also see Fig. 4, Table S5). This is because that the N_{CCN} was
275 calculated based on a constant S rather than refer to the availability of water vapor, while the
276 calculation of N_d is based on the S_{max} that can reach in the real atmosphere at a given updraft velocity.
277 In the cloud, the change in the quantity of cloud particles can be directly reflected by the change in
278 S_{max}. As shown in Fig. 2e, the average S_{max} for the two vertical updraft velocity of V=0.3 m s^{-1} and
279 V=2.1 m s^{-1} was calculated to be under 0.2% and 0.4%, varying largely with the variation of N_{CN} due
280 to the effect of water vapor competition, which will be discussed in Section 3.3.

281 **3.2 Quantitative evaluation of the NPF impact on N_{CCN} and N_d**

282 Based on the method in Section 2.4, the contribution of the NPF to N_{CCN} and N_d is calculated
283 and shown in Fig. 3. The results show that the N_{CCN} is averagely increased by 32.0%, 43.0%, 53.0%,
284 and 65.0% at S of 0.2%, 0.4%, 0.6% and 0.8% respectively during NPF events (Fig. 3b, c, Table S3),
285 amounting to about 24%-37% of environment CCN at the cloud-relevant supersaturation are directly
286 originated from NPF during the studied period in urban Beijing. And the rest (about 63-76%) of
287 CCN are from the other sources or pre-existing particles, which is much larger than that derived in
288 remote Finokalia, Crete, Greece by Kalkavouras et al (2019). In other words, due to the higher
289 background concentration of aerosol particles in polluted urban area, the relative contribution of NPF
290 to N_{CCN} is more significant in remote clean regions.

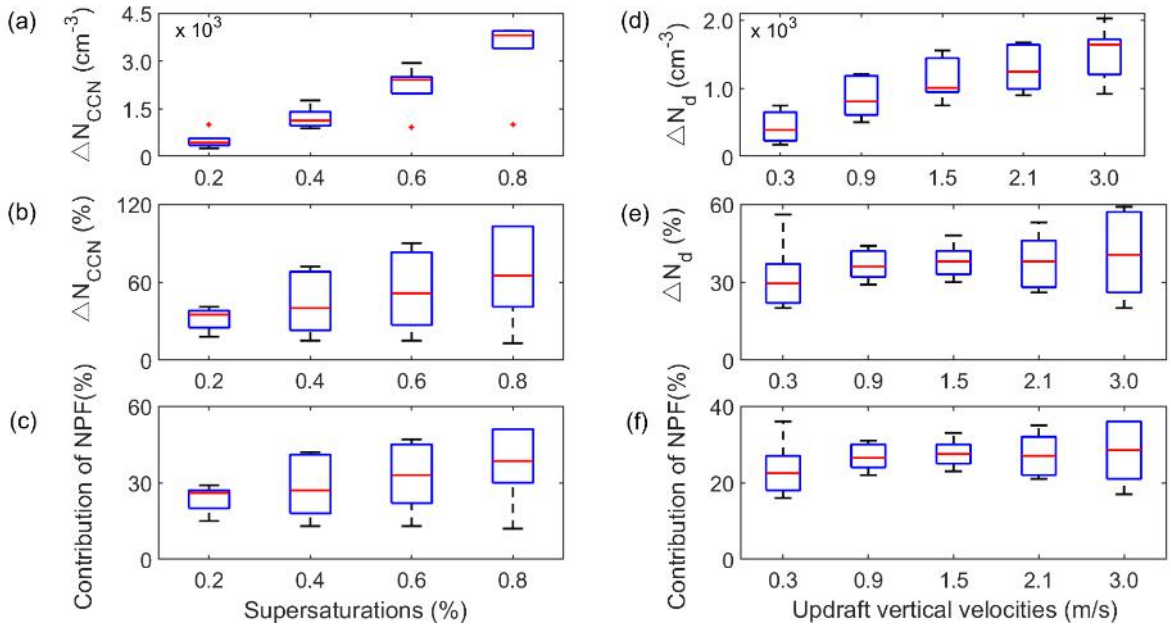

Figure 3. Box diagram of the increment of (a) CCN number concentration N_{CCN} (ΔN_{CCN}), (b) enhanced percentage of N_{CCN} and (c) the contribution to total N_{CCN} by NPF for different supersaturations (0.2%-0.8%), and (d) cloud droplet number concentration N_d (ΔN_d), (e) enhanced percentage of N_d and (f) the contribution to total N_d by NPF under different updraft velocities (0.3 m/s-3.0 m/s).

The estimated results of N_d for selected vertical updraft velocity are shown in Fig. 3d-f. Generally, the average S_{max} was calculated to be under 0.4% and 0.2% for V=2.1 m s^{-1} and V=0.3 m s^{-1} respectively (Fig. 2e), corresponding to critical particle sizes (d_c) of ~70 nm and ~110 nm. It means that most activated drops are from accumulation-mode particles and larger particles in Aitken-mode. The large contribution of the Aitken-mode particles leads to large amount of cloud droplets in urban Beijing, especially for high updraft velocity. Basically, the averaged ΔN_d (increased by NPF) are 433, 854, 1117, 1281, and 1523 cm^{-3} at updraft velocities of 0.3, 0.9, 1.5, 2.1, and 3 m s^{-1} respectively (Fig. 3d), which is a much larger magnitude compared with that in the clean areas (Morales et al., 2014; Sullivan et al.,2016; Kalkavouras et al., 2019). This is equal to that the N_d are enhanced by 32%, 37%, 38%, 38%, 40% at updraft velocities of 0.3, 0.9, 1.5, 2.1, and 3 m s^{-1} respectively (Fig. 3e),

suggesting that the higher cloud updraft velocity not only generates more cloud droplets, but also induces larger enhancements in N_d. We also show that the NPF contributes about 30% to the total N_d during the studied period in urban Beijing (Fig. 3f). And the rest (about 70%) of cloud droplet are from the other sources or pre-existing particles. With the increase of the S, the percentages of NPF-initiated N_{CCN} and the contributions of the NPF to N_{CCN} increased more significantly than that for N_d with the increase of V. In other words, the percentages of NPF-initiated N_d and the contributions of the NPF to N_d are relatively independent on the variation of V. This is primarily due to the water vapor competition effect under very high CN number concentrations when calculating the N_d. Under high N_{CN}, the water vapor competition effect will lead to lower S_{max}, which is smaller than that the constant S for calculating N_{CCN}. Roughly, the N_d at V of 0.3-3 m/s corresponds to the N_{CCN} at S of 0.1%-0.5%, within which the percentages of ΔN_{CCN} and the contributions of the NPF to N_{CCN} don't change much either. The effect of water vapor competition will be further examined in the following section.

3.3 The effect of water vapor competition on evaluating N_d

Fig. 4 shows the scatter plots of correlations between N_{CN} and N_{CCN} at supersaturations of 0.6% and 0.8% and the correlations between N_{CN} and N_d under updraft vertical velocities of 2.1 m s^{-1} and 3.0 m s^{-1}. The N_{CCN} and N_{CN} were obviously linearly related, but the correlation between N_d and N_{CN} was non-linear. When shown as the average values with error bars, the N_d increase linearly as N_{CN} increase when the N_{CN} is below 15000, then the N_d began to decrease with the further increase of N_{CN}. This has been presented in previous studies (Nenes et al., 2001; Ramanathan et al., 2001; Sullivan et al., 2016), and was believed to be caused by the water vapor competition of the aerosol particles. Although the larger updraft velocities can achieve greater supersaturation in adiabatic ascending

clouds and more particles can be activated into cloud droplets, the water vapor competition still occurred when background aerosol particles increased to a certain number. This is fully suggested by the difference between the calculated N_{CCN} using the constant S and the N_d using the variable S_{max} in the air parcels. Because in the actual environment, it is often unable to achieve the sufficient supersaturation compared to the prescribed ones that are preset in the instrument. For example, the average S_{max} is lower than 0.5% at the maximum cloud updraft velocity of 3 m s^{-1} according to the calculation results in this study. Therefore, although NPF events may strongly increase N_{CCN}, the formed N_d are eventually limited by water vapor competition which determines the S_{max} that varies in the cloud. The S_{max} is related to the cloud formation dynamics and the aerosol levels in the region.

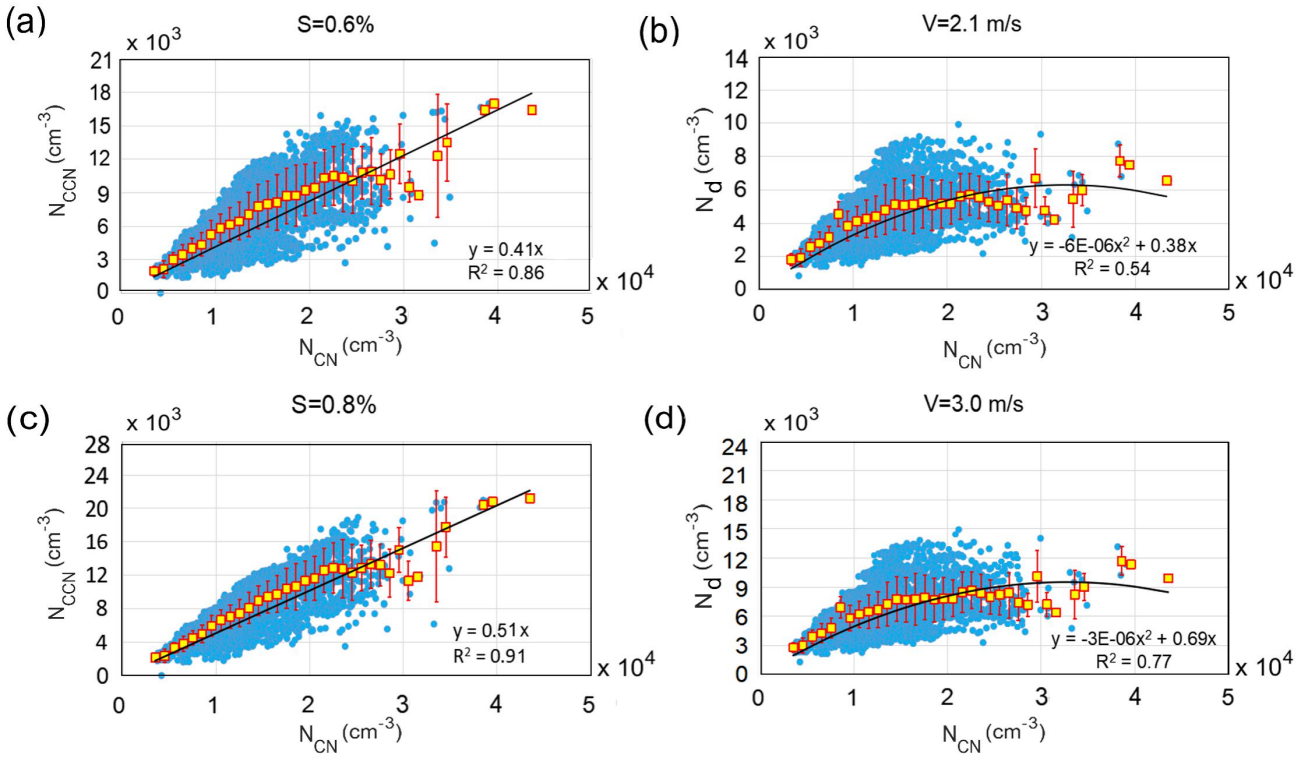

Figure 4. Scatter plots of correlation between total number concentration (N_{CN}) and CCN number concentration (N_{CCN}) at supersaturation of (a) 0.6% and (c) 0.8% respectively. Scatter plot of correlation between N_{CN} and cloud droplet number concentration (N_d) at updraft vertical velocity of

342 (b) 2.1 m s^{-1} and (d) 3.0 m s^{-1} respectively.

343 To evaluate the effect of water vapor competition on N_d, by taking the case on 11 June as an
344 example, we compare the N_d calculated from the varied S_{max} at different updraft velocities with the N_d
345 at referred constant S (Fig. 5). The results from other NPF cases were also summarized in Table S6
346 and Table S7. Obviously, after the t_{start}, the S_{max} starts to decrease and was negatively correlated with
347 N_d for both the updraft velocities, reflecting the enhanced effect of competition for water vapor from
348 the growing number of droplets (Fig. 5a and 5b). It is shown that S_{max} was decreased by 14.5±3.5%,
349 13.3±4.0%, 13.4±4.2%, 12.0±4.1%, 11.7±3.9% for V=0.3, 0.9, 1.5, 2.1 and 3 m s^{-1} respectively
350 (Fig. 5c, d).

351 Therefore, by compared to the N_d calculated from the constant S, the N_d calculated from the
352 variable S_{max} is greatly reduced at both the updraft velocities of 0.3 m s^{-1} and 2.1 m s^{-1} , suggesting a
353 significant suppression of cloud droplet formation. Quantitatively, the N_d are reduced by 19.0±4.5%,
354 15.7±4.7%, 14.8±5.6%, 12.3±4.9%, 11.8±5.0% at updraft velocity of 0.3, 0.9, 1.5, 2.1 and 3 m s^{-1}
355 respectively on the NPF days. Our results are similar with that reported by Kalkavouras et al., (2017),
356 which shows this competition effects suppress N_d by 20% for V = 0.3 m s^{-1} and 12.3 % for V = 0.6 m
357 s^{-1}. In addition, the declined percentages with increase of the updraft velocity suggests that the effect
358 becomes smaller at larger V that can achieve greater S_{max} in the environment. Essentially, water vapor
359 competition led to the reduction in N_d by decreasing the required S_{max} for the CN activation.

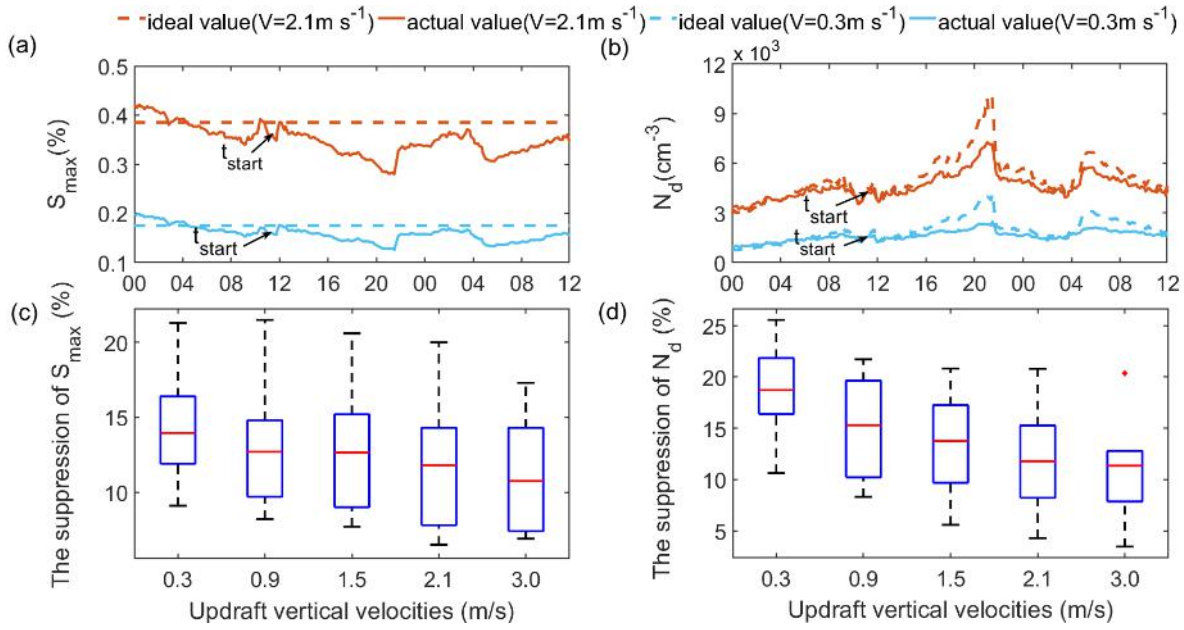

Figure 5. (a) The diurnal changes of the calculated maximum supersaturation (S_{max}) (referred to the constant supersaturation S) at V=0.3 m/s and 2.1 m/s on 11 June 2017; (b) Comparison of the cloud droplets number concentration (N_d) under the constant S and S_{max} on 11 June 2017; The suppression percentage of (c) S_{max} and (d) N_d due to the competition of water vapor.

3.4 The variations of CCN and cloud droplet on typical "clean" and "polluted" NPF day: a case study

Generally, the lower $PM_{2.5}$ means low background condensation sink (CS) which is conductive for the condensation and coagulation of nucleation particles (Wu et al., 2011; Yue et al., 2011; Wiedensohler et al., 2012). Different from the remote clean area, some of the NPF events in urban Beijing during the campaign occurred with background pollutions (with daily mass concentrations of $PM_{2.5}$ of ~40 μg m^{-3}) or are impacted by local primary emissions. This kind of NPF event has different characteristics from that in clean conditions, as the sudden increase of nucleation particles less than 25 nm is often accompanied by an increase of large particles at the beginning of NPF. Here, they are named as "polluted" and "clean" NPF event respectively. Two days, on 27 May and 11 June, representing the typical "polluted" and "clean" NPF events respectively, are selected for contrasting

the effect of the two kinds of NPF on CCN and CDNC. As shown in Fig. 7, there is a higher pre-existing background of accumulation mode particles across the day on "polluted" NPF day of 27 May than that on "clean" NPF day of 11 June. On "clean" NPF day, much more nucleation and Aitken mode particles, with N_{CN} enhancement of 2-fold higher than that on "polluted" day (Fig. 7a), were generated and NPF events developed stronger in the initial stage. The beginning of NPF events (t_{start}) on polluted case (11:00 a.m.) was about 2 hours later than that on clean case (~9:00 a.m).

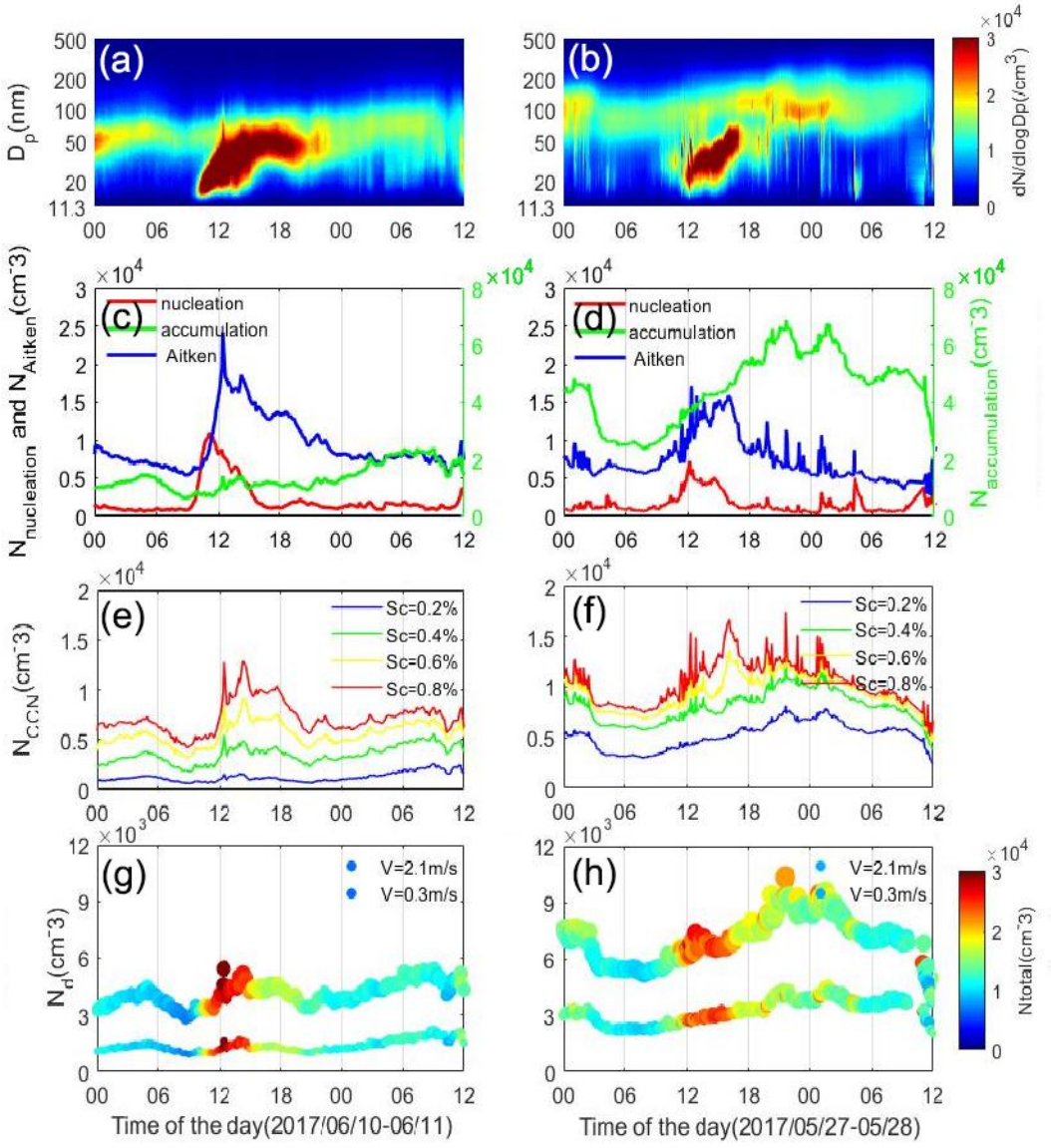

Figure 6. Comparison of (a, b) the particle number size distribution PNSD, (c, d) aerosol particle number concentration N_{CN}, (e, f) CCN number concentration N_{CCN} and (g, h) cloud droplet number

concentration N_d between a clean and a polluted NPF event. The "clean" NPF day is with a clean background ($PM_{2.5}$=14 (μg/m^3), and the "polluted" NPF day is with $PM_{2.5}$ of 73 μg/m^3.

For the both cases, the N_{CCN} are increased with the evolution of the NPF events (Fig. 6a, b, e, f). But the magnitude of the enhancements at the two cases are quite different. The N_{CCN} during NPF events under polluted day was generally twice than that of clean day (Fig. 6e and 6f), because there were a large number of pre-existing CCN-size aerosol particles on polluted NPF days. As a result, a larger increment of N_{CCN} is derived on clean NPF day, showing 37-80% and 15-41% increases percentage of N_{CCN} from NPF on clean and polluted days respectively (Fig. 7b). As for N_d, on clean days are 22% and 37%, and 34% and 26% on polluted days under updraft velocity of 0.3 and 2.1 m s^{-1}. The increase percentages in N_d between clean and polluted days are comparable. The result just further illustrates that the effect of water vapor competition on N_d under high N_{CN} in polluted atmosphere. This suggests that it is critical to fully consider the background meteorological conditions (e.g. using dynamic water vapor under different updraft velocities) to simulate the N_d when evaluating the effect of NPF on clouds and the associated climate effects.

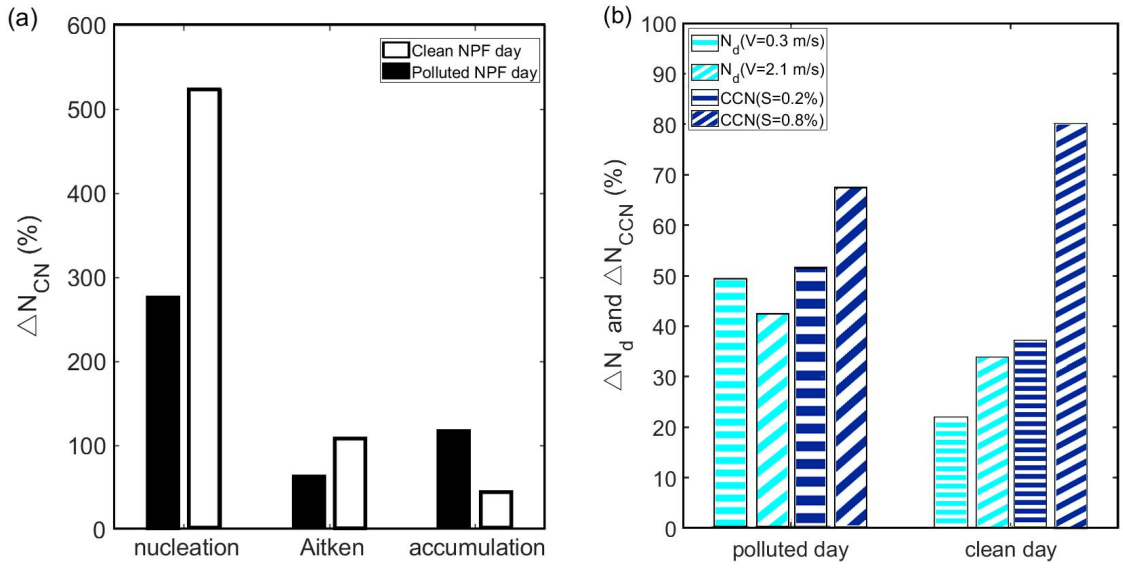

Figure 7. Comparison of the increments of (a) total particle number concentration (N_{CN}), and (b)

CCN number concentration (N_{CCN}) and cloud dropet number concentration (N_d) between the two different typical NPF events.

3.5 The impact of primary emissions during evening rush hour on the calculation of NPF contribution to N_{CCN} and N_d: *a case study*

During the campaign, very high number concentrations of fine particles were observed during evening rush hour (as shown in Fig.2a) when primary emissions related to automobile exhaust or cooking activities near the site may impact the PNSD. Those particles from primary emissions can serve as CCN and thereby impact the evaluation of NPF contribution to N_d. Therefore, taking the day of June 11 as an example, such effect from primary emissions during evening rush hour is investigated (Fig. 8). On the day, one hour after the burst of newly formed particles at ~12:00 a.m, the N_d began to rise rapidly, and the increase of N_d continued until to 21:30 at night (Fig. 1f). At ~18:00, the primary emissions also begin to impact the N_{CCN} and N_d. Note that a sudden decrease and dilution in the PNSD is due to a precipitation event at ~21:30. From 18:00-21:30, the CCN and cloud droplets were from both NPF source and the primary emissions. The impact of primary emissions is also indicated by the variations of particles composition during 18:00-22:00, when both the primary organic aerosols (POA) and BC show a rapid increase in the mass concentration and fraction (Fig. 8c and 8d). Here, a positive matrix factorization (PMF) analysis was performed to separate the primary and secondary organic aerosol factors quantitatively for the purpose of source apportionment based on field measurement by a Aerodyne high-resolution time-of-flight aerosol mass spectrometer (HR-ToF-AMS) (Xu et al., 2017; Zhang et al., 2011). The PMF algorithm in the robust mode (Paatero and Tapper, 1994) was applied to the high-resolution mass spectra to resolve distinct OA factors representing primary and secondary sources and processes. More details about operation of the

HR-ToF-AMS and PMF analysis also can be found in support information of Liu et al., (2021).

To evaluate the impact of the primary emissions, it is critical to separate the particle modes representing the primary aerosols from the observed PNSD. According to the observed characteristics of PNSD, the newly formed particles continue to grow and dominated by Aitken mode for several hours after the NPF occurred (Fig. 8a). The size mode of the newly formed particles during the rush hour is estimated by applying a growth rate of 3.2±0.5 nm h^{-1}, which is calculated by the variation of median particle size during 12:00-18:00. The calculation results show that the NPF-tracked particles can grow to ~50-60 nm during the rush hour period. While, the primary particles from vehicles or cooking are generally with a smaller size (~30 nm) than the NPF-tracked particles mode and accumulation mode (~100-120 nm) according to Brines et al. (2015) (Dall'Osto, et al., 2011; Harrison, et al., 2011), so we applied three modes to fit the PNSD from the beginning of the evening rush hour to the end assuming a normal distribution. Note that the size mode for background aerosols almost coincides with the accumulation mode of primary emitted particles during the period. Since the mode and concentration of background aerosols do not change much before and after the occurrence of new particles (Fig. 8a, b), the impact of background aerosol is thus deducted from the fitting accumulation mode. The fitted result shows a major peak in the Aitken mode at ~50 nm that is related to the NPF event, and two minor peaks in Aitken (~30 nm) and accumulation (~100-120 nm) mode (Fig. 8e, f) that are associated with the primary vehicle or cooking emissions. Fig. 8g and Fig. 8h show the separated PNSD of the NPF-related and primary aerosols respectively. Then the increment of N_{CCN} and N_d from NPF are obtained from the PNSD of NPF mode, and the increment of N_{CCN} and N_d from primary emissions are obtained by subtracting the increment of N_{CCN} and N_d by NPF from the total increment of N_d.

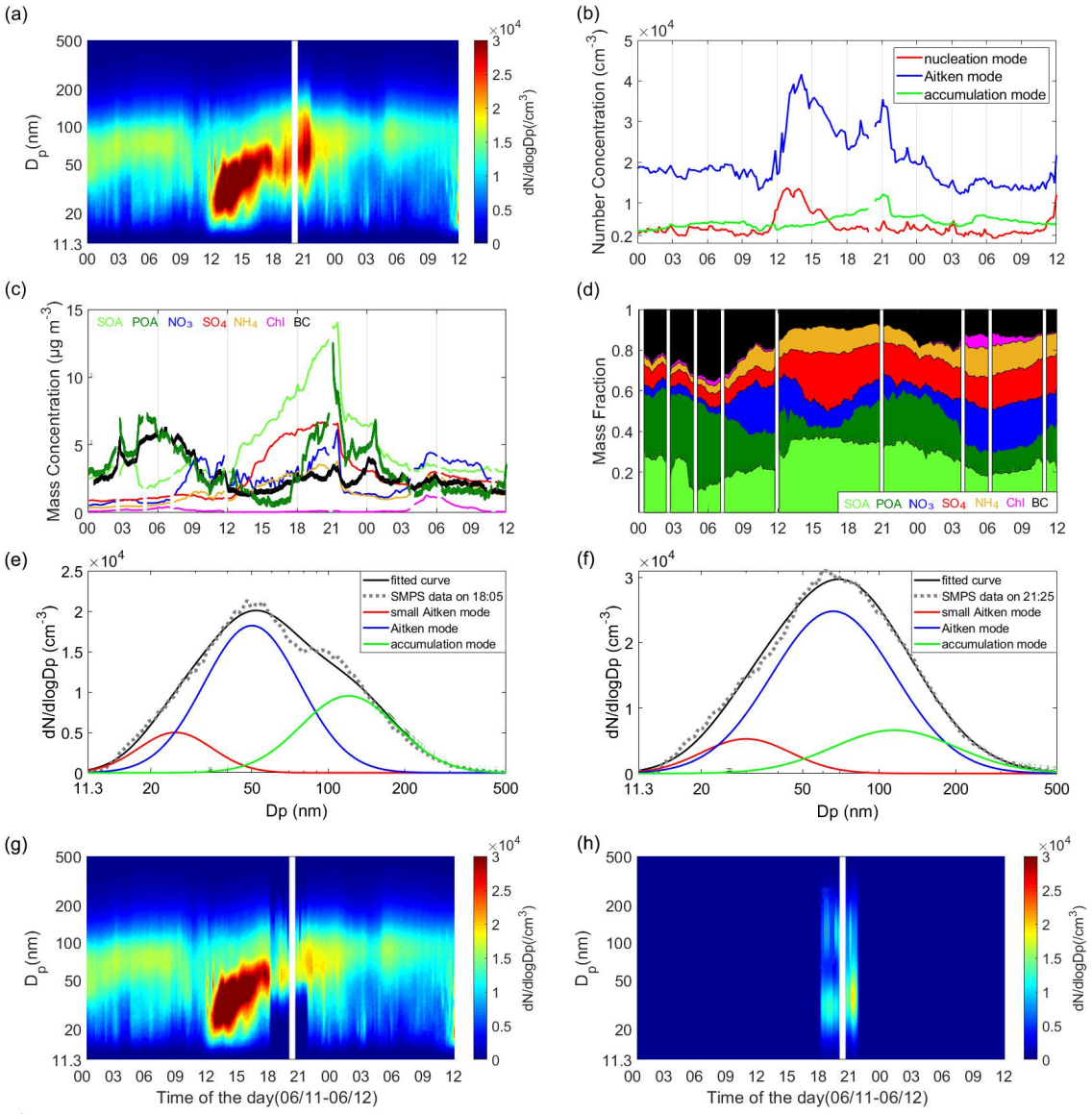

Figure 8. Diurnal variations of the (a) aerosol size distribution, (b) particle number concentrations for different size modes, (c) mass concentrations of aerosol chemical composition, and (d) mass fraction of aerosol chemical components, (e) (f) fitted three modes of the particle number concentration PNSD at 18:00 and 21:30, and (g) diurnal variations of the separated NPF-related PNSD and (h) the PNSD of primary aerosols.

Table 2. Quantitative evaluation of the contribution of primary emissions to N_d and N_{CCN}

V or S	D_c	$\triangle N_{d\_NPF}$ or ΔN_{CCN_NPF}		$\triangle N_{d\_PE}$ [a] or ΔN_{CCN_PF} [a]		$\triangle N_{d\_total}$ or $\triangle N_{CCN\_total}$
$m\ s^{-1}$,or %	nm	cm^{-3},	%	cm^{-3},	%	cm^{-3}
Evaluation of the contribution of primary emissions to N_d						
0.3	140	200	84.4%	37	15.6%	237
0.9	107	543	86.6%	84	13.4%	627
1.5	93	676	87.5%	97	12.5%	773
2.1	84	750	83.1%	153	16.9%	903
3.0	75	942	77.1%	279	22.9%	1221
Evaluation of the contribution of primary emissions to N_{CCN}						
0.2%	109	654	92.0%	57	8.0%	711
0.4%	69	1356	87.2%	199	12.8%	1555
0.6%	52	1680	87.1%	249	12.9%	1929
0.8%	43	1801	85.0%	318	15.0%	2119

[a]PE, primary emission

The calculated results are summarized in Table 2. For N_d, the average contribution of primary emission to N_d is 15.6%, 13.4%, 12.5%, 16.9% and 22.9% cm^{-3} for updraft velocities of 0.3, 0.9, 1.5, 2.1 and 3 m s^{-1} respectively. The proportion of contribution from NPF and primary emission to N_d increment change with the variation of V. The higher proportion of contribution from primary emission is obtained at higher V, which may be determined by the different characteristics between atmospheric particles emitted from the evening traffic sources and generated from NPF events. For N_{CCN}, the average contribution from primary emissions is 8.0%, 12.8%, 12.9%, 15.0% at S of 0.2%, 0.4%, 0.6%, 0.8% respectively. Compared with N_d, the contribution percentage of primary emission to N_{CCN} is smaller due to that the total N_{CCN} is much more than the total N_d. Our result shows considerable impact of those primary sources when evaluating the NPF contribution to cloud droplet number, highlighting the importance of considering the influence from multiple (i.e. secondary and primary) sources on clouds in the polluted atmosphere. Finally, it is worth noting that the dynamic changes of PBL would also impact the N_{CCN} and N_d during the period, and the decrease in the height

of PBL from the daytime to evening will result in an increase of N_{CCN} or N_d. However, for this case, the impact from primary emissions is much more prominent as indicated by the sharply raised particle number concentrations during the rush hour (Fig. 8b).

4 Conclusions

In this study, we quantified the contribution of NPF to N_d at typical updraft velocities in clouds using field measurements of aerosol number size distributions and chemical composition in urban Beijing. We show that the NPF drives the variations of N_{CCN} and N_d. About 32%-65% N_{CCN} are increased by NPF events for supersaturation 0.2%-0.8% in polluted atmosphere. And the N_d is increased about 32%-40% by NPF at V= 0.3-3 m s^{-1} accordingly. The significant reduction in N_d is observed due to water vapor competition with consideration of actual environmental updraft velocity, with decrease rates of 11.8%±5.0% at V=3 m $s^{-1}$and 19.0%±4.5% at V=0.3 m s^{-1} by comparing with that from a constant supersaturation. The effect of water vapor competition becomes smaller at larger V at which the greater S_{max} can be achieved. Essentially, water vapor competition led to the reduction in N_d by decreasing the environmental S_{max} for the activation of aerosol particles. It is shown that S_{max} was decreased by 14.5 $\pm$ 3.5% to 11.7 $\pm$ 3.9% for V=0.3-3 m s^{-1}. Our results suggest significant suppression of cloud droplet formation due to the water vapor competition particularly at extremely high aerosol particle number concentrations. As a result, although a larger enhancement of CCN-size particles by NPF event is derived on clean NPF day when there are few pre-existing background aerosol particles, no large discrepancy in the enhancement of N_d by NPF between the clean and polluted NPF day. Finally, we show a considerable impact of the primary sources when evaluating the NPF contribution to cloud droplet number from a case study. Our study highlights the importance of fully consideration of both the environmental meteorological conditions and multiple sources (i.e.

secondary and primary) to evaluate the effect of NPF on clouds and the associated climate effects. For example, Merikanto et al. 2010 used model to simulate the variation of CDNC from the year of 1850 to 2000, and showed that NPF made a nearly equal contribution (16-13.5%) to global CDNC in all those years, leading to about 50% enhancement in the year from1850 to 2000 change in cloud albedo. There are still large uncertainties about how to accurate quantitatively assess the response of these climate effects to NPF. This study is carried out in polluted urban area, which is a supplement to the research of the microphysical process of aerosol-cloud and provides a new perspective for the follow-up research in urban atmosphere. Note that, there are still limitations of our studies, as we only investigated several NPF cases within a short period due to the limited measurement data. The small sample size might cause bias in the results. Further studies based on more measurement data, i.e. with longer time periods and more observational sites, warrant to verify and refine our results, so as to parameterize the impact of NPF events on cloud, precipitation, and radiative forcing in models.

Acknowledgments

This work was supported by the National Basic Research Program of China (2017YFC1501702), the National Natural Science Foundation of China (Grants 41675141, 41975174). All data used in the study are available on https://data.mendeley.com/datasets/hkkzbn4zv3/1 or from the corresponding author upon request (fang.zhang@bnu.edu.cn).

Author statement

The authors declare no competing financial interest.

Author contribution

FZ and SJ conceived the conceptual development of the paper. LC, YS and JR contributed measurements. SJ directed and performed the experiments with LC, JL, JR, XY, ZL and FZ, SJ conducted the data analysis and wrote the draft of the paper. All authors commented on the paper.

References

Albrecht, B. A.: Aerosols, cloud microphysics, and fractional cloudiness, Science, 245, 1227–1230, 1989.

Altstädter, B., Platis, A., Wehner, B., Scholtz, A., Wildmann, N., Hermann, M., Käthner, R., Baars, H., Bange, J., and Lampert, A.: ALADINA – an unmanned research aircraft for observing vertical and horizontal distributions of ultrafine particles within the atmospheric boundary layer. Atmos. Meas. Tech., 8, 1627–1639, https://doi.org/10.5194/amt-8-1627-2015, 2015.

Abdul-Razzak, H., Ghan, S., and Rivera-Carpio, C.: A parametreization of aerosol activation: 1. Single aerosol types, J. Geophys. Res., 103, 6123–6131, 1998.

Abdul-Razzak, H. and Ghan, S.: A parametreization of aerosol activation: 2. Multiple aerosol types, J. Geophys. Res., 105, 6837–6844, 2000.

Asmi, E., Kivekäs, N., Kerminen, V.-M., Komppula, M., Hyvärinen, A. P., Hatakka, J., Viisanen, Y., and Lihavainen, H.: Secondary new particle formation in Northern Finland Pallas site between the years 2000 and 2010, Atmos. Chem. Phys., 11, 12959–12972, https://doi.org/10.5194/acp-11-12959-2011, 2011.

Boucher, O. and Lohmann, U.: The sulfate-CCN-cloud albedo effect, Tellus, 47B, 281–300, 1995.

Bousiotis, D., Dall'Osto, M., Beddows, D. C. S., Pope, F. D., and Harrison, R. M.: Analysis of new particle formation (NPF) events at nearby rural, urban background and urban roadside sites, Atmos. Chem. Phys., 19, 5679–5694, https://doi.org/10.5194/acp-19-5679-2019, 2019.

Brines, M., Dall'Osto, M., Beddows, D. C. S., Harrison, R. M., Gómez-Moreno, F., Núñez, L., Artíñano, B., Costabile, F., Gobbi, G. P., Salimi, F., Morawska, L., Sioutas, C., and Querol, X.: Traffic and nucleation events as main sources of ultrafine particles in high-insolation developed world cities, Atmos. Chem. Phys., 15, 5929–5945, https://doi.org/10.5194/acp-15-5929-2015, 2015.

Cai, M., Liang, B., Sun, Q., Zhou, S., Chen, X., Yuan, B., Shao, M., Tan, H., and Zhao, J.: Effects of continental emissions on cloud condensation nuclei (CCN) activity in the northern South China Sea during summertime 2018, Atmos. Chem. Phys., 20, 9153–9167, https://doi.org/10.5194/acp-20-9153-2020, 2020.

Collins, D. R., Flagan, R. C., and Seinfeld, J. H.: Improved inversion of scanning DMA data, Aerosol Sci. Tech., 36, 1–9, 2002.

Dal, M., Kulmala, M., Riipinen, I., Wagner, R., Hussein, T., Aalto, P. P., and Lehtinen, K. E. J.: Formation and growth of fresh atmospheric aerosols: eight years of aerosol size distribution data from SMEAR II, Hyytiälä, Finland, Boreal Environ. Res., 10, 323–336, 2005.

Dall'Osto, M., Thorpe, A., Beddows, D. C. S., Harrison, R. M., Barlow, J. F., Dunbar, T., Williams, P. I., and Coe, H.: Remarkable dynamics of nanoparticles in the urban atmosphere, Atmos. Chem. Phys., 11, 6623–6637, https://doi.org/10.5194/acp-11-6623-2011, 2011.

Duan, J., Wang, Y., Xie, X., Li, M., Tao, J., Wu, Y., Cheng, T.: Influence of pollutants on activity of aerosol cloud condensation nuclei (CCN) during pollution and post-rain periods in Guangzhou, southern China, Science of the Total Environment, 642, 1008-1019, 10.1016/j.scitotenv.2018.06.053, 2018.

Fan, J., Leung, R., Rosenfeld, D., Chen, Q., Li, Z., Zhang, J., and Yan, H.: Microphysical effects determine macrophysical response for aerosol impacts on deep convective clouds, P. Natl. Aacad. Sci. USA, 110, E4581–E4590, https://doi.org/10.1073/pnas.1316830110, 2013.

Fan, X., Liu, J., Zhang, F., Chen, L., Collins, D., Xu, W., Jin, X., Ren, J., Wang, Y., Wu, H., Li, S., Sun, Y., and Li,

Z.: Contrasting size-resolved hygroscopicity of fine particles derived by HTDMA and HR-ToF-AMS measurements between summer and winter in Beijing: the impacts of aerosol aging and local emissions, Atmos. Chem. Phys., 20, 915–929, https://doi.org/10.5194/acp-20-915-2020, 2020.

Fountoukis, C. and Nenes, A.: Continued development of a cloud droplet formation parameterization for global climate models, J. Geophys. Res., 110, D11212, https://doi.org/10.1029/2004JD005591, 2005.

Genz, C., Schrödner, R., Heinold, B., Henning, S., Baars, H., Spindler, G., and Tegen, I.: Estimation of cloud condensation nuclei number concentrations and comparison to in situ and lidar observations during the HOPE experiments, Atmos. Chem. Phys., 20, 8787–8806, https://doi.org/10.5194/acp-20-8787-2020, 2020.

Ghan, S., Chung, C., and Penner, J.: A parameterization of cloud droplet nucleation part I: single aerosol type, Atmos. Res., 30, 198–221, https://doi.org/10.1016/0169-8095(93)90024-I, 1993.

Gunthe, S. S., King, S. M., Rose, D., Chen, Q., Roldin, P., Farmer, D. K., Jimenez, J. L., Artaxo, P., Andreae, M. O., Martin, S. T., and Pöschl, U.: Cloud condensation nuclei in pristine tropical rainforest air of Amazonia: size-resolved measurements and modeling of atmospheric aerosol composition and CCN activity, Atmos. Chem. Phys., 9, 7551–7575, https://doi.org/10.5194/acp-9-7551-2009, 2009.

Harrison, R. M., Beddows, D. and Dall'Osto, M.: PMF Analysis of Wide-Range Particle Size Spectra Collected on a Major Highway, Environmental Science & Technology, 45(14), 5522, 10.1021/es201998m, 2011.

Hudson, J. G. , Noble, S., and Tabor, S.: Cloud supersaturations from CCN spectra hoppel minima. Journal of Geophysical Research Atmospheres, 120(8), 3436–3452. https://doi.org/10.1002/2014JD022669, 2015.

Kalkavouras, P., Bossioli, E., Bezantakos, S., Bougiatioti, A., Kalivitis, N., Stavroulas, I., Kouvarakis, G., Protonotariou, A. P., Dandou, A., Biskos, G., Mihalopoulos, N., Nenes, A., and Tombrou, M.: New particle formation in the southern Aegean Sea during the Etesians: importance for CCN production and cloud droplet number, Atmos. Chem. Phys., 17, 175–192, https://doi.org/10.5194/acp-17-175-2017, 2017.

575 Kalkavouras, P. , Bougiatioti, A. , Kalivitis, N. , Stavroulas, I. , and Mihalopoulos, N.: Regional new particle
576 formation as modulators of cloud condensation nuclei and cloud droplet number in the eastern mediterranean.
577 Atmos. Chem. Phys., 19(9), 6185-6203, https://doi.org/10.5194/acp-19-6185-2019,2019.
578 Kazil, J., Stier, P., Zhang, K., Quaas, J., Kinne, S., O'Donnell, D., Rast, S., Esch, M., Ferrachat, S., Lohmann, U.,
579 Feichter, J.: Aerosol nucleation and its role for clouds and Earth's radiative forcing in the aerosol-climate model
580 ECHAM5-HAM, Atmos. Chem. Phys., 10, 10733, https://doi.org/10.5194/acp-10-10733-2010, 2010.
581 Kerminen, V. M., Paramonov, M., Anttila, T., Riipinen, I., Fountoukis, C., Korhonen, H., Asmi, E., Laakso, L.,
582 Lihavainen, H., Swietlicki, E., Svenningsson, B., Asmi, A., Pandis, S. N., Kulmala, M., and Petäjä, T.: Cloud
583 condensation nuclei production associated with atmospheric nucleation: a synthesis based on existing literature
584 and new results, Atmos. Chem. Phys., 12, 12037-12059, https://doi.org/10.5194/acp-12-12037-2012, 2012.
585 Kerminen, V. M., Chen, X., Vakkari, V., Petäjä, T., Kulmala, M., and Bianchi, F.: Atmospheric new particle
586 formation and growth: review of field observations, Environ. Res. Lett., 13, 103003,
587 https://doi.org/10.1088/1748-9326/aadf3c, 2018.
588 Khvorostyanov, V. I., and Curry, J. A.: A simple analytical model of aerosol properties with account for hygroscopic
589 growth: 1. Equilibrium size spectra and cloud condensation nuclei activity spectra, J. Geophys. Res., 104,
590 2175-2184, https://doi.org/10.1029/98JD02687, 1999.
591 Köhler, H.: The nucleus in and the growth of hygroscopic droplets, Transactions of the Faraday Society, 32:
592 1152-1161, https://doi.org/10.1039/tf9363201152, 1936.
593 Kulmala, M. and Kerminen, V. M.: On the formation and growth of atmospheric nanoparticles, Atmos. Res., 90,
594 132–150, https://doi.org/10.1016/j.atmosres.2008.01.005, 2008.
595 Kulmala, M., Petäjä, T., Nieminen, T., Sipilä, M., Manninen, H. E., Lehtipalo, K., Dal, Maso, M., Aalto, P.,
596 Junninen, H., Paasonen, P., Riipinen, I., Lehtinen, K. E. J., Laaksonen, A., and Kerminen, V.-M.: Measurement of

597 the nucleation of atmospheric aerosol particles, Nat. Protocol., 7, 1651–1667,
598 https://doi.org/10.1038/nprot.2012.091, 2012.
599 Leaitch, W. R., Strapp, J. W., and Isaac, G. A.: Cloud droplet nucleation and cloud scavenging of aerosol sulphate
600 in polluted atmospheres, Tellus, 38B, 328–344, https://doi.org/10.1111/j.1600-0889.1986.tb00258.x ,1986
601 Leino, K., Nieminen, T., Manninen, H. E., Petäjä, T., Kerminen, V. M., and Kulmala, M.: Intermediate ions as a
602 strong indicator of new particleformation bursts in a boreal forest, Boreal Environ. Res., 21, 274-286, 2016.
603 Li Y., Zhang F., Li Z., Sun L., Wang Z., Li P., Sun Y., Ren J., Wang Y. and Cribb M.: Influences of aerosol
604 physiochemical properties and new particle formation on CCN activity from observation at a suburban site of
605 China, Atmos. Res., 188, 80-89, https://doi.org/10.1016/j.atmosres.2017.01.009,2017.
606 Li, Z., Niu, F., Fan, J. et al. Long-term impacts of aerosols on the vertical development of clouds and precipitation.
607 Nature Geosci 4, 888–894 ,https://doi.org/10.1038/ngeo1313, 2011.
608 Li, Z., Guo, J., Ding, A., Liao, H., Liu, J., Sun, Y., Wang, T., Xue, H., Zhang, H., and Zhu, B.: Aerosols and
609 boundary-layer interactions and impact on air quality. Natl. Sci. Rev., 4, 810–833,
610 https://doi.org/10.1093/nsr/nwx117, 2017.
611 Liu, C., Wang, T., Rosenfeld, D., Zhu, Y., Yue, Z., Yu, X.: Anthropogenic effects on cloud condensation nuclei
612 distribution and rain initiation in East Asia. Geophysical Research Letters, 47,
613 https://doi.org/10.1029/2019GL086184,2019.
614 Liu, J., Zhang, F., Xu, W., Sun, Y., Chen, L., Li, S.: Hygroscopicity of organic aerosols linked to formation
615 mechanisms. Geophysical Research Letters, 48, https://doi.org/10.1029/2020GL091683, 2021.
616 Ma, N., Zhao, C., Tao, J., Wu, Z., Kecorius, S., Wang, Z., Größ, J., Liu, H., Bian, Y., Kuang, Y., Teich, M., Spindler,
617 G., Müller, K., van Pinxteren, D., Herrmann, H., Hu, M., and Wiedensohler, A.: Variation of CCN activity during
618 new particle formation events in the North China Plain, Atmos. Chem. Phys., 16, 8593–8607,

https://doi.org/10.5194/acp-16-8593-2016, 2016.

Martin, G., Johnson, D.: The measurement and parameterization of effective radius of droplets in warm stratocumulus clouds.[J]. Journal of the Atmospheric Sciences, https://doi.org/10.1175/1520-0469(1994)051<1823: TMAPOE>2.0.CO;2,1994.

Merikanto, J., Spracklen, D. V., Pringle, K. J., and Carslaw, K. S.: Effects of boundary layer particle formation on cloud droplet number and changes in cloud albedo from 1850 to 2000, Atmos. Chem. Phys., 10, 695–705, https://doi.org/10.5194/acp-10-695-2010, 2010.

Morales, R. and Nenes, A.: Characteristic updrafts for computing distribution-averaged cloud droplet number and stratocumulus cloud properties, J. Geophys. Res., 115, D18220, https://doi.org/10.1029/2009JD013233, 2010.

Morales, R., Nenes, A.: Understanding the contributions of aerosol properties and parameterization discrepancies to droplet number variability in a global climate model. Atmos Chem Phys 14(9):4809–4826,2014.

Nenes, A., Chan, S., Abdul-Razzak, H., Chuang, P., and Seinfeld, J. H.: Kinetic limitations on cloud droplet formation and impact on cloud albedo, Tellus 53B, 133–149, https://doi.org/10.3402/tellusb.v53i2.16569, 2001.

Nenes, A. and Seinfeld, J. H.: Parameterization of cloud dropletformation in global climate models, J. Geophys. Res, 108, 4415, https://doi.org/10.1029/2002JD002911, 2003.

Ng, N. L., Herndon, S. C., Trimborn, A., Canagaratna, M. R., Croteau, P. L., Onasch, T. B.: An aerosol chemical speciation monitor (ACSM) for routine monitoring of the composition and mass concentrations of ambient aerosol, Aerosol Science and Tech, 45(7): 780-794, https://doi.org/10.1080/02786826.2011.560211, 2011.

Paasonen, P. and TAPPER, U.: Positive matrix factorization: A nonnegative factor model with optimal utilization of error-estimates of data values, Journal Citation Reports, 5: 112-126, 10.1002/env.3170050203, 1994.

Paasonen, P., Peltola, M., Kontkanen, J., Junninen, H., Kerminen, V.-M., and Kulmala, M.: Comprehensive analysis of particle growth rates from nucleation mode to cloud condensation nuclei in boreal forest, Atmos. Chem. Phys.,

641 18, 12085–12103, https://doi.org/10.5194/acp-18-12085-2018, 2018.
642 Peng, J. F., Hu, M., Wang, Z. B., Huang, X. F., Kumar, P., Wu, Z. J., Guo, S., Yue, D. L., Shang, D. J., Zheng, Z.,
643 and He, L. Y.: Submicron aerosols at thirteen diversified sites in China: size distribution, new particle formation
644 and corresponding contribution to cloud condensation nuclei production, Atmos. Chem. Phys., 14, 10249–10265,
645 https://doi.org/10.5194/acp-14-10249-2014, 2014.
646 Peng,Y., Dong, Y., Li, X. M.: Different Characteristics of New Particle Formation Events at Two Suburban Sites in
647 Northern China. Atmosphere, 8(12), 258, https://doi.org/10.3390/atmos8120258, 2017.
648 Petters, M. D. and Kreidenweis, S. M.: A single parameter representation of hygroscopic growth and cloud
649 condensation nucleus activity, Atmos. Chem. Phys., 7, 1961–1971, https://doi.org/10.5194/acp-7-1961-2007,
650 2007.
651 Ramanathan, V., Crutzen, P. J., Kiehl, J. T., and Rosenfeld, D.: Aerosols, climate, and the hydrological cycle,
652 Science, 294, 2119–2124, https://doi.org/10.1126/science.1064034, 2001.
653 Ren, J., Zhang, F., Wang, Y., Collins, D., Fan, X., Jin, X., Xu, W., Sun, Y., Cribb, M., and Li, Z.: Using different
654 assumptions of aerosol mixing state and chemical composition to predict CCN concentrations based on field
655 measurements in urban Beijing, Atmos. Chem. Phys., 18, 6907–6921, https://doi.org/10.5194/acp-18-6907-2018,
656 2018.
657 Rose, C., Sellegri, K., Moreno, I., Velarde, F., Ramonet, M., Weinhold, K., Krejci, R., Andrade, M., Wiedensohler,
658 A., Ginot, P., and Laj, P.: CCN production by new particle formation in the free troposphere, Atmos. Chem.
659 Phys., 17, 1529–1541, https://doi.org/10.5194/acp-17-1529-2017, 2017.
660 Seinfeld, J. H., Bretherton, C. S., Carslaw, K. S., Coe, H., DeMott, P. J., Dunlea, E. J., Feingold, G., Ghan, S. J.,
661 Guenther, A.B., Kahn, R. A., Kracunas, I. P., Kreidenweis, S. M., Molina, M. J., Nenes, A., Penner, J. E., Prather,
662 K. A., Ramanathan, V., Ramaswamy, V., Rasch, P. J., Ravishankara, A. R., Rosenfeld, D., Stephens, G., and

663 Wood R.: Improving Our Fundamental Understanding of the Role of Aerosol-Cloud Interactions in the Climate
664 System, P. Nat. Acad. Sci. USA, 113, 5781–5790, https://doi.org/10.1073/pnas.1514043113, 2016.
665 Shi, J., Khan, A., Harrison, R.: Measurements of ultrafine particle concentration and size distribution in the urban
666 atmosphere, Science of the Total Environment, 235(1-3):51-64, https://doi.org/10.1016/S0048-9697 (99)00189-8,
667 1999.
668 Spracklen, D. V., Carslaw, K. S., Merikanto, J., Mann, G. W., Reddington, C. L., Pickering, S., Ogren, J. A.,
669 Andrews, E., Baltensperger, U., Weingartner, E., Boy, M., Kulmala, M., Laakso, L., Lihavainen, H., Kivekäs, N.,
670 Komppula, M., Mihalopoulos, N., Kouvarakis, G., Jennings, S. G., O'Dowd, C., Birmili, W., Wiedensohler, A.,
671 Weller, R., Gras, J., Laj, P., Sellegri, K., Bonn, B., Krejci, R., Laaksonen, A., Hamed, A., Minikin, A., Harrison,
672 R. M., Talbot, R., and Sun, J.: Explaining global surface aerosol number concentrations in terms of primary
673 emissions and particle formation, Atmos. Chem. Phys., 10, 4775–4793,
674 https://doi.org/10.5194/acp-10-4775-2010, 2010.
675 Stanier, C., Khlystov, A., Pandis, S.: Ambient aerosol size distributions and number concentrations measured during
676 the Pittsburgh Air Quality Study (PAQS), Atmospheric Environment, 38(20):3275-3284, https://doi.org/10.1016/
677 j.atmosenv.2004.03.020, 2004.
678 Sullivan, S. C., Lee, D., Oreopoulos, L., and Nenes, A.: The role of updraft velocity in temporal variability of cloud
679 hydrometeor number, P. Natl. Acad. Sci. USA, 113, 5781–5790, https://doi.org/10.1073/pnas.1514043113, 2016.
680 Sun, Y. L., Wang, Z. F., Du, W., Zhang, Q., Wang, Q. Q., Fu, P. Q., Pan, X. L., Li, J., Jayne, J., and Worsnop, D. R.:
681 Longterm real-time measurements of aerosol particle composition in Beijing, China: seasonal variations,
682 meteorological effects, and source analysis, Atmos. Chem. Phys., 15, 10149–10165,
683 https://doi.org/10.5194/acp-15-10149-2015, 2015.
684 Tao, J., Kuang, Y., Ma, N., Hong, J., Sun, Y., Xu, W., Zhang, Y., He, Y., Luo, Q., Xie, L., Su, H., and Cheng, Y.:

685 Secondary aerosol formation alters CCN activity in the North China Plain, Atmos. Chem. Phys., 21, 7409–7427,
686 https://doi.org/10.5194/acp-21-7409-2021, 2021.
687 Twomey, S.: The influence of pollution on the shortwave albedo of clouds, J. Atmos. Sci., 34, 1149–1152, 1977.
688 Wang, S. C. and Flagan, R. C.: Scanning Electrical Mobility Spectrometer, Aerosol Sci. Tech., 13, 230–240, 1990.
689 Wang Y., Zhang F., Li Z., Tan H., Xu H., Ren J., Zhao J., Du W. and Sun Y.: Enhanced hydrophobicity and
690 volatility of submicron aerosols under severe emission control conditions in Beijing, Atmos Chem Phys, 17,
691 5239-5251, https://doi.org/10.5194/acp-17-5239-2017, 2017.
692 Wiedensohler, A., Birmili, W., Nowak, A., Sonntag, A., Weinhold, K., Merkel, M., Wehner, B., Tuch, T., Pfeifer, S.:
693 Mobility particle size spectrometers: harmonization of technical standards and data structure to facilitate high
694 quality long-term observations of atmospheric particle number size distributions, Atmos. Meas. Tech., 5,
695 657–685, https://doi.org/10.5194/amt-5-657-2012, 2012.
696 Wiedensohler, A., Chen, Y. F., Nowak, A., Wehner, B., Achtert, P., Berghof, M., Birmili, W., Wu, Z. J., Hu, M., Zhu,
697 T., Takegawa, N., Kita, K., Kondo, Y., Lou, S. R., Hofzumahaus, A., Holland, F., Wahner, A., Gunthe, S. S., Rose,
698 D., Su, H., and Pöschl, U.: Rapid aerosol particle growth and increase of cloud condensation nucleus activity by
699 secondary aerosol formation and condensation: A case study for regional air pollution in northeastern China, J.
700 Geophys. Res., 114, D00G08, https://doi.org/10.1029/2008JD010884, 2008.
701 Wu, Z., Hu, M., Liu, S., Wehner, B., and Wiedensohler, A.: Particle number size distribution in the urban
702 atmosphere of Beijing, China, Atmos. Environ., 42, 7967–7980, 2008.
703 Wu, Z. J., Hu, M., Yue, D. L.: Evolution of particle number size distribution in an urban atmosphere during
704 episodes of heavy pollution and new particle formation. Sci China Earth Sci, 2011, 54, https://doi.org/
705 10.1007/s11430-011-4227-9,2011.
706 Wu, Z. J., Poulain, L., Birmili, W., Größ, J., Niedermeier, N., Wang, Z. B., Herrmann, H., and Wiedensohler, A.:

Some insights into the condensing vapors driving new particle growth to CCN sizes on the basis of hygroscopicity measurements, Atmos. Chem. Phys., 15, 13071–13083, https://doi.org/10.5194/acp-15-13071-2015, 2015.

Xu, W. Q., Han, T. T., Du, W., Wang, Q. Q., Chen, C., Zhao, J.: Effects of aqueous-phase and photochemical processing on secondary organic aerosol formation and evolution in Beijing, China. Environmental Science & Technology, 51(2), 762 – 770. https://doi.org/10.1021/acs.est.6b04498, 2017.

Yue, D. L., Hu, M., Zhang, R. Y., Wu, Z. J., Su, H., Wang, Z. B., Peng, J. F., He, L. Y., Huang, X. F., Gong, Y. G., Wiedensohler, A.: Potential contribution of new particle formation to cloud condensation nuclei in Beijing[J]. Atmospheric Environment, 2011, 45(33):6070-6077, https://doi.org/10.1016/j.atmosenv.2011.07.037.

Zimmerman, A. , Petters, M. D. , & Meskhidze, N.: Observations of new particle formation, modal growth rates, and direct emissions of sub-10 nm particles in an urban environment. Atmospheric Environment, 242, 117835.

Zhang, Q., Jimenez, J. L., Canagaratna, M. R., Ulbrich, I. M., Ng, N. L., Worsnop, D. R., and Sun, Y. L.: Understanding atmospheric organic aerosols via factor analysis of aerosol mass spectrometry: A review. Analytical and Bioanalytical Chemistry, 401(10), 3045–3067. https://doi.org/10.1007/s00216-011-5355-y, 2011.

Zhang, F., Li, Y., Li, Z., Sun, L., Li, R., Zhao, C., Wang, P., Sun, Y., Liu, X., Li, J., Li, P., Ren, G., and Fan, T.: Aerosol hygroscopicity and cloud condensation nuclei activity during the AC3Exp campaign: implications for cloud condensation nuclei parameterization, Atmos. Chem. Phys., 14, 13423–13437, https://doi.org/10.5194/acp-14-13423-2014, 2014.

Zhang, F., Li, Z., Li, Y., Sun, Y., Wang, Z., Li, P., Sun, L., Wang, P., Cribb, M., Zhao, C., Fan, T., Yang, X., and Wang, Q.: Impacts of organic aerosols and its oxidation level on CCN activity from measurement at a suburban site in China, Atmos. Chem. Phys., 16, 5413–5425, https://doi.org/10.5194/acp-16-5413-2016, 2016.

Zhang, F., Wang, Y., Peng, J., Ren, J., Collins, D., Zhang, R., Li, Z.: Uncertainty in predicting CCN activity of aged

729 and primary aerosols. Journal of Geophysical Research: Atmospheres, 122, 11,723–11,736.
730 https://doi.org/10.1002/2017JD027058, 2017.
731 Zhang, F., Ren, J., Fan, T., Chen, L., Xu, W., Sun, Y.: Significantly enhanced aerosol CCN activity and number
732 concentrations by nucleation-initiated haze events: A case study in urban Beijing. J. Geophys. Res.-Atmos., 124.
733 https://doi.org/10.1029/ 2019JD031457, 2019
734 Zheng, Y. T.,Rosenfeld, D.,Li, Z. Q.: Satellite Inference of Thermals and Cloud-Base Updraft Speeds Based on
735 Retrieved Surface and Cloud-Base Temperatures, Journal of the Atmospheric Sciences,2015,72(6),
736 https://doi.org/10.1175/JAS-D-14-0283.1,2015.